UC Irvine
UC Irvine Previously Published Works

Title

The lipid elongation enzyme ELOVL2 is a molecular regulator of aging in the retina

Permalink

Journal

ISSN

Authors

Chen, Daniel
Chao, Daniel L
Rocha, Lorena
et al.

Publication Date

DOI

Peer reviewed

ORIGINAL ARTICLE

Aging Cell WILEY

The lipid elongation enzyme ELOVL2 is a molecular regulator of aging in the retina

Daniel Chen[1] | Daniel L. Chao[1] | Lorena Rocha[1] | Matthew Kolar[2] | Viet Anh Nguyen Huu[1] | Michal Krawczyk[1] | Manish Dasyani[1] | Tina Wang[3] | Maryam Jafari[1] | Mary Jabari[1] | Kevin D. Ross[4] | Alan Saghatelian[2] | Bruce A. Hamilton[4,5] | Kang Zhang[1] | Dorota Skowronska-Krawczyk[1,6] (ID)

[1]Shiley Eye Institute, Viterbi Family Department of Ophthalmology, University of California San Diego, La Jolla, CA, USA

[2]The Salk Institute for Biological Studies, Clayton Foundation Laboratories for Peptide Biology, La Jolla, CA, USA

[3]Department of Medicine, University of California San Diego, La Jolla, CA, USA

[4]Department of Cellular and Molecular Medicine, University of California San Diego, La Jolla, CA, USA

[5]Institute for Genomic Medicine, University of California San Diego, La Jolla, CA, USA

[6]Atkinson Laboratory for Regenerative Medicine, University of California San Diego, La Jolla, CA, USA

Correspondence
Dorota Skowronska-Krawczyk, Shiley Eye Institute, Viterbi Family Department of Ophthalmology, University of California, San Diego, 9500 Gilman Drive, La Jolla, CA 92093, USA.
Email: DorotaSK@health.ucsd.edu

Funding information
NIH, Grant/Award Number: R01 EY02701, R01 GM086912, K12 EY024225, T32 GM008; UCSD Vision Research Center Core

Abstract

Methylation of the regulatory region of the elongation of very-long-chain fatty acids-like 2 (*ELOVL2*) gene, an enzyme involved in elongation of long-chain polyunsaturated fatty acids, is one of the most robust biomarkers of human age, but the critical question of whether *ELOVL2* plays a functional role in molecular aging has not been resolved. Here, we report that *Elovl2* regulates age-associated functional and anatomical aging in vivo, focusing on mouse retina, with direct relevance to age-related eye diseases. We show that an age-related decrease in *Elovl2* expression is associated with increased DNA methylation of its promoter. Reversal of *Elovl2* promoter hypermethylation in vivo through intravitreal injection of 5-Aza-2'-deoxycytidine (5-Aza-dc) leads to increased *Elovl2* expression and rescue of age-related decline in visual function. Mice carrying a point mutation C234W that disrupts *Elovl2*-specific enzymatic activity show electrophysiological characteristics of premature visual decline, as well as early appearance of autofluorescent deposits, well-established markers of aging in the mouse retina. Finally, we find deposits underneath the retinal pigment epithelium in *Elovl2* mutant mice, containing components found in human drusen, a pathologic hallmark of age related macular degeneration. These findings indicate that ELOVL2 activity regulates aging in mouse retina, provide a molecular link between polyunsaturated fatty acids elongation and visual function, and suggest novel therapeutic strategies for the treatment of age-related eye diseases.

KEYWORDS
age-related macular degeneration, aging, DNA methylation, ELOVL2, retina, PUFA

Chen and Chao authors contributed equally

- -

1 | INTRODUCTION

Chronological age predicts relative levels of mental and physical performance, disease risks across common disorders, and mortality (Glei, 2016). The use of chronological age is limited, however, in explaining the considerable biological variation among individuals of a similar age. Biological age is a concept that attempts to quantify different aging states influenced by genetics and a variety of environmental factors. While epidemiological studies have succeeded in providing quantitative assessments of the impact of discrete factors on human longevity, advances in molecular biology now offer the ability to look beyond population-level effects and to hone in on the effects of specific factors on aging within single organisms.

A quantitative model for aging based on genome-wide DNA methylation patterns by using measurements at 470,000 CpG markers from whole-blood samples of a large cohort of human individuals spanning a wide age range has recently been developed (Hannum, 2013; Horvath, 2013; Levine, 2018). This method is highly accurate at predicting age and can also discriminate relevant factors in aging, including gender, genetic variants, and disease (Gross, 2016; Hannum, 2013). Several models work in multiple tissues (Horvath, 2013; Levine, 2018), suggesting the possibility of a common molecular clock, regulated in part by changes in the methylome. In addition, these methylation patterns are strongly correlated with cellular senescence and aging (Xie, Baylin, & Easwaran, 2019). The regulatory regions of several genes become progressively methylated with increasing chronological age, suggesting a functional link between age, DNA methylation, and gene expression. The promoter region of *ELOVL2*, in particular, was the first to be shown to reliably show increased methylation as humans age (Garagnani, 2012), and confirmed in one of the molecular clock models (Hannum, 2013).

ELOVL2 (elongation of very-long-chain fatty acids-like 2) encodes a transmembrane protein involved in the elongation of long-chain (C22 and C24) omega-3 and omega-6 polyunsaturated fatty acids (LC-PUFAs; Leonard, 2002). Specifically, ELOVL2 is capable of converting docosapentaenoic acid (DPA) (22:5n-3) to 24:5n-3, which can lead to the formation of very-long-chain PUFAs (VLC-PUFAs) as well as 22:6n-3, docosahexaenoic acid (DHA; Gregory, Cleland, & James, 2013). DHA is the main polyunsaturated fatty acid in the retina and brain. Its presence in photoreceptors promotes healthy retinal function and protects against damage from bright light and oxidative stress. *ELOVL2* has been shown to regulate levels of DHA (Pauter, 2014), which in turn has been associated with age-related macular degeneration (AMD), among a host of other retinal degenerative diseases (Bazan, Molina, & Gordon, 2011). In general, LC-PUFAs are involved in crucial biological functions including energy production, modulation of inflammation, and maintenance of cell membrane integrity. It is, therefore, possible that *ELOVL2* methylation plays a role in the aging process through the regulation of these diverse biological pathways.

In this study, we investigated the role of ELOVL2 in molecular aging in the retina. We find that the *Elovl2* promoter region is increasingly methylated with age in the retina, resulting in age-related decreases in *Elovl2* expression. These changes are associated with decreasing visual structure and function in aged mice. We then demonstrate that loss of ELOVL2-specific function results in the early-onset appearance of sub-RPE deposits that contain molecular markers found in drusen in AMD. This phenotype is also associated with visual dysfunction as measured by electroretinography, and it suggests that ELOVL2 may serve as a critical regulator of a molecular aging clock in the retina, which may have important therapeutic implications for diseases such as age-related macular degeneration.

2 | RESULTS

2.1 | Elovl2 expression is downregulated with age through methylation and is correlated with functional and anatomical biomarkers in aged wild-type mice

Previous studies showed that methylation of the promoter region of *ELOVL2* is highly correlated with human age (Hannum, 2013). Methylation of regulatory regions is thought to prevent the transcription of neighboring genes and serves as a method to regulate gene expression. We first wished to characterize whether the age-associated methylation of the *ELOVL2* promoter previously found in human serum also occurs in the mouse. First, we analyzed ELOVL2 promoter methylation data obtained using bisulfite sequencing in mouse blood and compared it to the available human data for the same region (Wang, 2017) and observed similar age-related increase in methylation level in the compared regions (Figure S1a). To assay methylation of the *Elovl2* promoter in retina, we used methylated DNA immunoprecipitation (MeDIP) method (Weber, 2005) and tested the methylation levels in the CpG island in the *Elovl2* regulatory region by quantitative PCR with *Elovl2*-specific primers (Table S1). MeDIP analysis of the CpG island in the *Elovl2* regulatory region showed increasing methylation with age in the mouse retina (Figure 1a). This was well-correlated with age-related decreases in expression of *Elovl2* as assessed by Western blot and qPCR (Figure 1b and Figure S1b,c) indicating the potential role of age-related changes in DNA methylation in *Elovl2* expression.

To understand the cell-type and age-specific expression of *Elovl2*, we performed in situ hybridization with an *Elovl2* RNAscope probe on mouse retina sections (Stempel, Morgans, Stout, & Appukuttan, 2014). In three-month-old and in 22-month-old mice, we noticed *Elovl2* expression in the photoreceptor layer, particularly in the cone layer as well as the RPE (Figure 1c and Figure S1e). We observed that the expression of Elovl2 on mRNA level in RPE was lower than in the retina (Figure S1d). Importantly, at older stages (22-month-old animals), we noticed *Elovl2* mRNA in the same locations but dramatically reduced in expression (Figure 1c). As *Elovl2* is also highly expressed in the liver, we performed a time course of *Elovl2* expression in this tissue. We observed similar age-related decreases in *Elovl2* expression correlated with increases in methylation of the *Elovl2* promoter in mouse liver, indicating that age-associated methylation of *Elovl2* occurs in multiple tissues in mice (Figure S1f).

Visual function is highly correlated with age, including age-related decreases in rod function in both humans and mice (Birch & Anderson,

FIGURE 1 ELOVL2 expression is downregulated with age through methylation of its promoter and is correlated with age-related increases in autofluorescence aggregates and decreased scotopic response. (a) Methylation of ELOVL2 promoter region measured using immunoprecipitation of methylated (MeDIP) followed by qPCR. ELOVL2 promoter is increasingly methylated with age. (b) Time course of retinal ELOVL2 protein expression by Western blot. ELOVL2 protein is expression decreases with age. ns, nonspecific signal produced by ELOVL2 antibodies (c) Images of mouse retina sections from young—3mo (top panels) and old—22mo (bottom panels) animals stained with RNAscope probes designed for *Elovl2* and *Arrestin 3*, counterstained with DAPI. ONL, outer nuclear layer, INL, inner nuclear layer, RGC, retinal ganglion cells. Bar—100um. (d) Time course of representative fundus autofluorescence pictures of C57BL/6J mice. Arrows denote autofluorescent deposits. (e) Quantification of autofluorescent deposits in fundus images. $N = 4$. (f) Scotopic responses by ERG over mouse lifespan. For panels A, E, and F, $N = 4$, $*p < .5$, $**p < .01$, 1-way ANOVA. Error bars denote SD
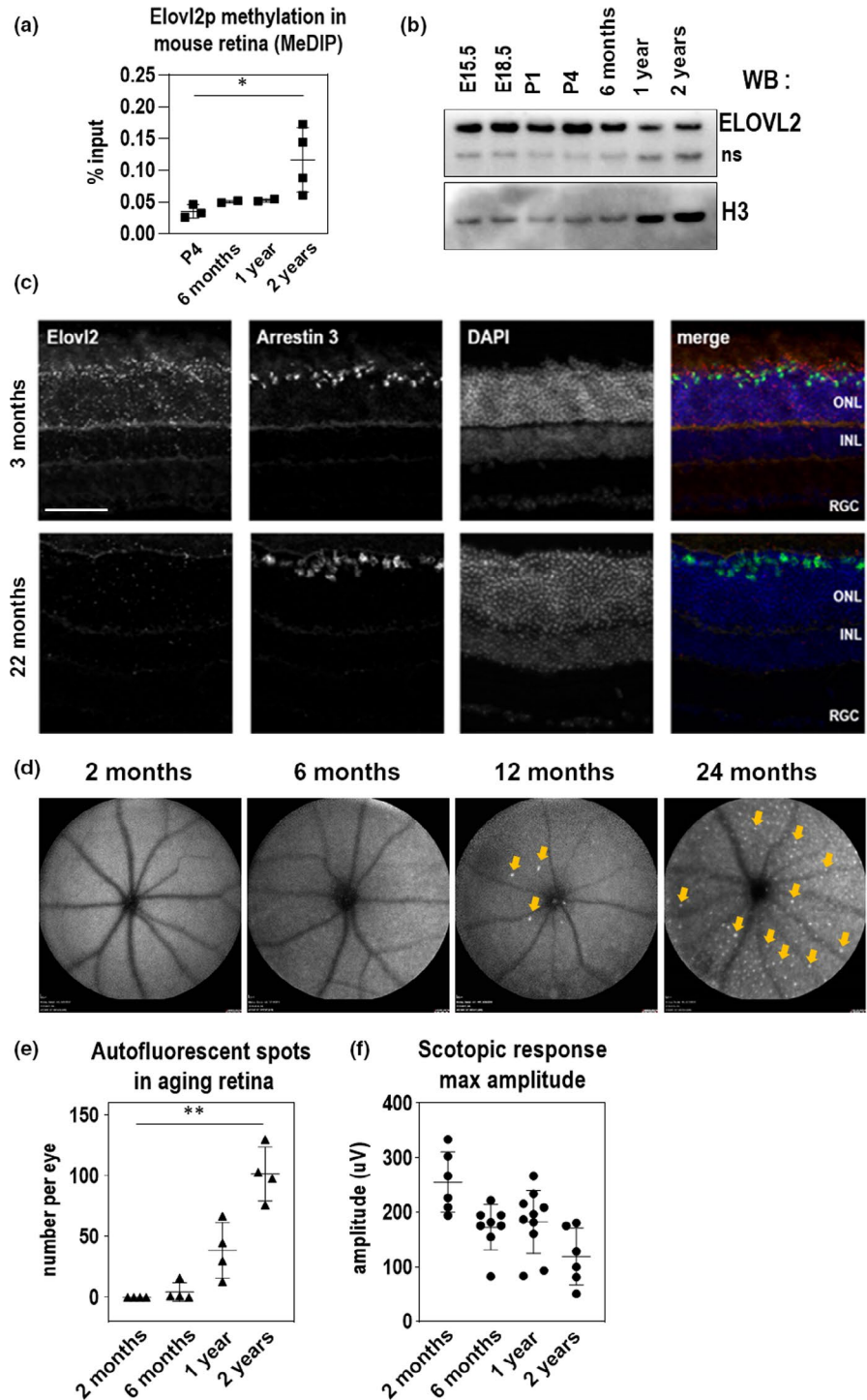
1992; Kolesnikov, Fan, Crouch, & Kefalov, 2010). In addition, autofluorescent aggregates have been observed in the fundus of aged mice, suggesting that these aggregates may also be an anatomical surrogate of aging in the mouse retina (Chavali, 2011; Xu, Chen, Manivannan, Lois, & Forrester, 2008). To measure and correlate these structural and visual function changes with age in mice, we performed an analysis of wild-type C57BL/6J mice at various timepoints through development, using fundus autofluorescence and electroretinography (ERG) as structural and functional readouts for vision. We observed increasing amounts of autofluorescent aggregates on fundus autofluorescence imaging with increasing mouse age, most prominently at two years (Figure 1d,e and Figure S1g). We also detected an age-associated decrease in visual function, as measured by maximum scotopic amplitude by ERG (Figure 1f and Figure S1h), as shown in previous studies (Kolesnikov et al., 2010; Williams & Jacobs, 2007). These data show that an age-associated accumulation of autofluorescent spots and decrease in visual function as detected by ERG correlate with *Elovl2* downregulation in the mouse retina.

2.2 | Manipulating ELOVL2 expression causes age-related changes in cells

The WI38 and IMR90 cell lines are well-established cell models of aging (Hayflick, 1965). We used these cell lines to further explore the effect of *ELOVL2* promoter methylation on cell health. First, using MeDIP, we found that promoter methylation increased with cell population doubling (Figure 2a) further confirming strong correlation

between increased *ELOVL2* methylation and aging. Since the methylation of the promoter region was shown to be inhibitory for transcription (Jones, 1998), we investigated whether the expression level of *ELOVL2* inversely correlated with *ELOVL2* promoter methylation. Using qRT–PCR, we found that the expression level of the gene decreased with increasing population doubling (PD) number (Figure 2b). We conclude that *ELOVL2* expression is downregulated in aging cells, with a correlated increase in *ELOVL2* promoter methylation.
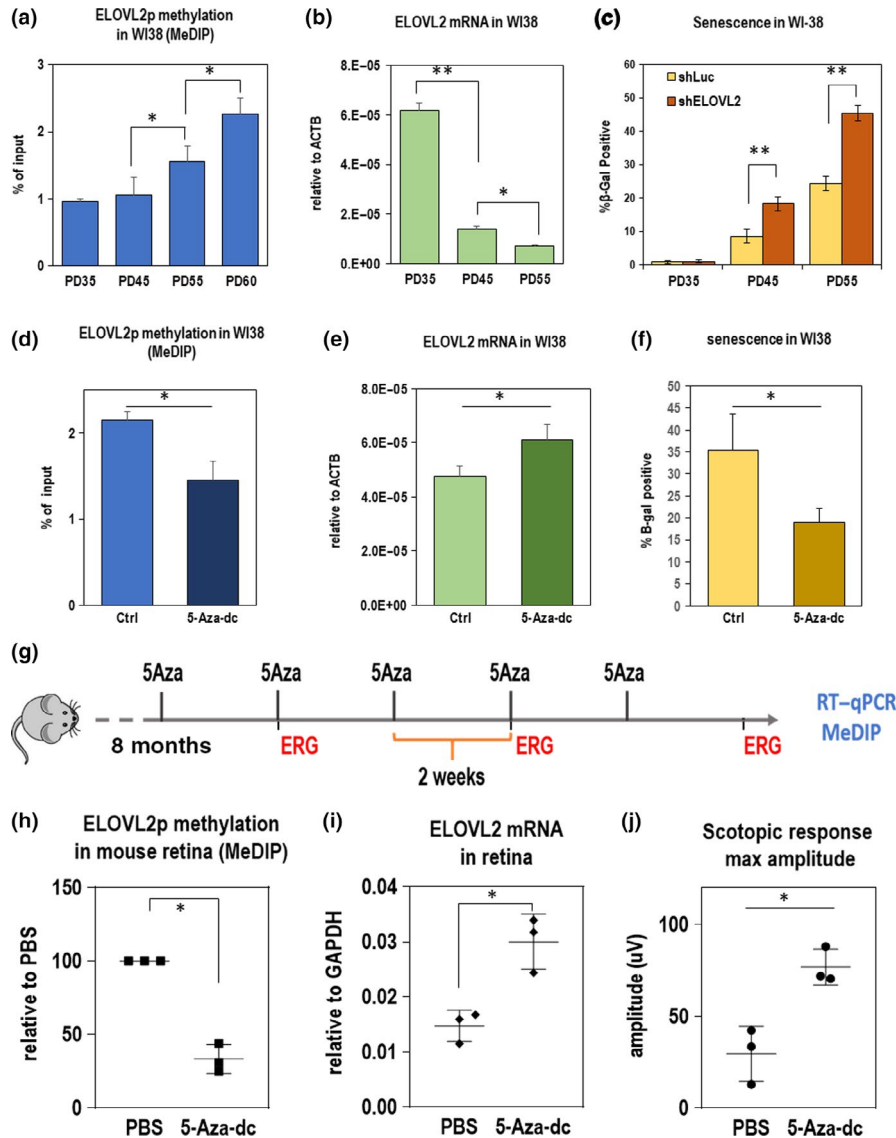

FIGURE 2 (a-c) *ELOVL2* expression, methylation, and senescence in WI38 csells. (a) Methylation level in *ELOVL2* promoter region in human normal lung cell line WI38 by MeDIP/qPCR. Amplicons contain CpG markers cg16867657, cg24724428, and cg21572722. N > 3. (b) *ELOVL2* expression by qPCR in WI38 cells at PD35, PD45, and PD55. (c) Fraction of senescent cells measured by beta-galactosidase staining in WI38 cells at given population doubling upon shRNA-mediated knockdown of ELOVL2 gene or control Luc. (d-f) Manipulating DNA methylation in PD52 WI38 cells. (d) *ELOVL2* promoter methylation as measured by MeDIP followed by qPCR in untreated control and 5-Aza-dc-treated WI38 cells. (e) *ELOVL2* expression by qPCR in untreated control and 5-Aza-dc-treated WI38 cells. (f) Percent senescence by beta-galactosidase staining in WI38 cells treated with 2µM 5-Aza-dc. (g-j) Manipulating DNA methylation in mice. (g) Experimental setup. Eight-month-old mice were injected intravitreally with 5-Aza-dc five times every two weeks. ERG measurements were taken at indicated time points. At 11 months, expression and methylation levels were measured in 5-Aza-dc treated and control (PBS-treated) mice. (h) Methylation of ELOVL2 promoter by MeDIP at 11 months after 5-Aza injection. (i) *ELOVL2* expression by qPCR after 5-Aza injection. (j) Maximum amplitude scotopic response by ERG after 5-Aza injection. For panels A-F, N>=3, *p < .05, **p < .01, t test. Error bars denote *SD*; for panels H-J, N = 3, *p < .05, **p < .01, t test. Error bars denote *SD*

We then asked whether modulating the expression of *ELOVL2* could influence cellular aging. First, using shRNA delivered by lentivirus, we knocked down *ELOVL2* expression in WI38 and another model cell line, IMR-90, and observed a significant decrease in proliferation rate (Figure S2a,b), an increased number of senescent cells in culture as detected by SA-β-gal staining (Figure 2c and Figure S2e), and morphological changes consistent with morphology of high PD cells (Figure S2f). Altogether, these data suggest that decreasing ELOVL2 expression results in increased aging and senescence in vitro.

Next, we tested whether we could manipulate *Elovl2* expression by manipulating the *Elovl2* promoter methylation. We treated WI38 fibroblasts with 5-Aza-2'-deoxycytidine (5-Aza-dc), a cytidine analog that inhibits DNA methyltransferase (Momparler, 2005). Cells were treated for two days with 2 μM 5-Aza-dc followed by a five-day washout period. Interestingly, we found that upon treatment with 5-Aza-dc, *Elovl2* promoter methylation was reduced (Figure 2d), and *Elovl2* expression was upregulated (Figure 2e). Moreover, upon 5-Aza-dc treatment, a lower percentage of senescent cells were observed in culture (Figure 2f). To assess whether the decrease in senescence is caused at least in part by the ELOVL2 function, we knocked down the *ELOVL2* expression in aged WI38 cells and treated them with 5-Aza-dc as previously described. Again, significantly lower proportion of senescent cells was detected upon the drug treatment, but the effect of drug treatment was significantly reduced by shRNA-mediated knockdown of *ELOVL2*, using either of two *ELOVL2* shRNAs compared with a control shRNA (Figure S2b). This indicates an important role of ELOVL2 in the process. Altogether, these data suggest that the reversing *ELOVL2* promoter methylation increases its expression and decreases senescence in vitro.

2.3 | DNA demethylation in the retina by intravitreal injection of 5-Aza-dc increases Elovl2 expression and rescues age-related changes in scotopic function in aged mice

We next explored whether demethylation of the *Elovl2* promoter could have similar effects on *Elovl2* expression in vivo. To accomplish this, we performed intravitreal injection of 5-Aza-dc, known to affect DNA methylation in nondividing neurons (Choi, Lee, Kim, Choi, & Lee, 2018; Christman, 2002; Miller & Sweatt, 2007; Wang, 2018), into aged wild-type mice. Eight-month-old C57BL/6J mice were injected with 1 μl of 2 μM 5-Aza-dc in one eye and 1 μl of PBS in the other eye as a control, every other week over a period of 3 months (total of 5 injections) (Figure 2g). After the treatment, tissues were collected, and RNA and DNA were extracted. We found, using the MeDIP method, that methylation of the *Elovl2* promoter decreased after treatment (Figure 2h), with a corresponding upregulation of *Elovl2* expression (Figure 2i). Notably, we observed that the scotopic response was significantly improved in the 5-Aza-dc-injected eyes compared with vehicle controls (Figure 2j). These data show that DNA demethylation, which included demethylation

of the *Elovl2* promoter region, influence and potentially delay age-related changes in visual function in the mouse retina.

2.4 | Elovl2^C234W mice demonstrate a loss of ELOVL2-specific enzymatic activity

We next sought to investigate the in vivo function of *Elovl2* in the retina. Since C57BL/6 *Elovl2* knockout heterozygous mice display defects in spermatogenesis and are infertile (Zadravec, 2011), we developed an alternative strategy to eliminate ELOVL2 enzymatic activity in vivo. Using CRISPR-Cas9 technology, we generated *Elovl2*-mutant mice encoding a cysteine-to-tryptophan substitution (C234W). This mutation selectively inactivates enzymatic activity of *ELOVL2* required to process C22 PUFAs, to convert docosapentaenoic acid (DPA) (22:5n-3) to 24:5n-3, while retaining elongase activity for other substrates common for ELOVL2 and the paralogous enzyme ELOVL5 (Figure 3a, Figure S3a; Gregory et al., 2013; Gregory et al., 2013; Zadravec, 2011). A single-guide RNA against the *Elovl2* target region, a repair oligonucleotide with a base pair mutation to generate the mutant C234W, and Cas9 mRNA were injected into C57BL/6N mouse zygotes (Figure 3b). One correctly targeted heterozygous founder with the C234W mutation was identified. No off-target mutations were found based on DNA sequencing of multiple related DNA sequences in the genome (Figure S3b). The C234W heterozygous mice were fertile, and C234W homozygous mice developed normally and showed no noticeable phenotypes. We analyzed the long-chain fatty levels in the retinas of homozygous *Elovl2*^C234W mice to determine whether there was a loss of enzymatic activity specific to ELOVL2. We observed that *Elovl2*^C234W mice had higher concentrations of C22:5 fatty acid (a selective substrate of ELOVL2 elongation) and lower levels of C24:5 (primary product of ELOVL2 enzymatic activity) and C22:6 (DHA—the secondary product of ELOVL2) (Figure 3c). We also observed similar changes in fatty acid levels in livers of *Elovl2*^C234W mice as well as lower levels of longer fatty acids that require primary product of Elovl2 as a substrate (Figure S4) This suggests that the *Elovl2*^C234W mice have altered ELOVL2 substrate specificity and inhibited ELOVL2-specific C22 elongase activity.

2.5 | Loss of ELOVL2-specific activity results in early vision loss and accumulation of sub-RPE deposits

We next investigated whether the *Elovl2*^C234W mutation affected the retinal structure and/or function in vivo. First, we observed a significant number of autofluorescent spots on fundus photography in animals at six months of age, which were not found in wild-type littermates (Figure 4a,b). This phenotype was consistently observed in 6-, 8-, and 12-month-old mutant animals and in both animal sexes, but the phenotype was consistently more pronounced in male mice (Figure S5). Importantly, ERG analysis revealed that 6-month-old
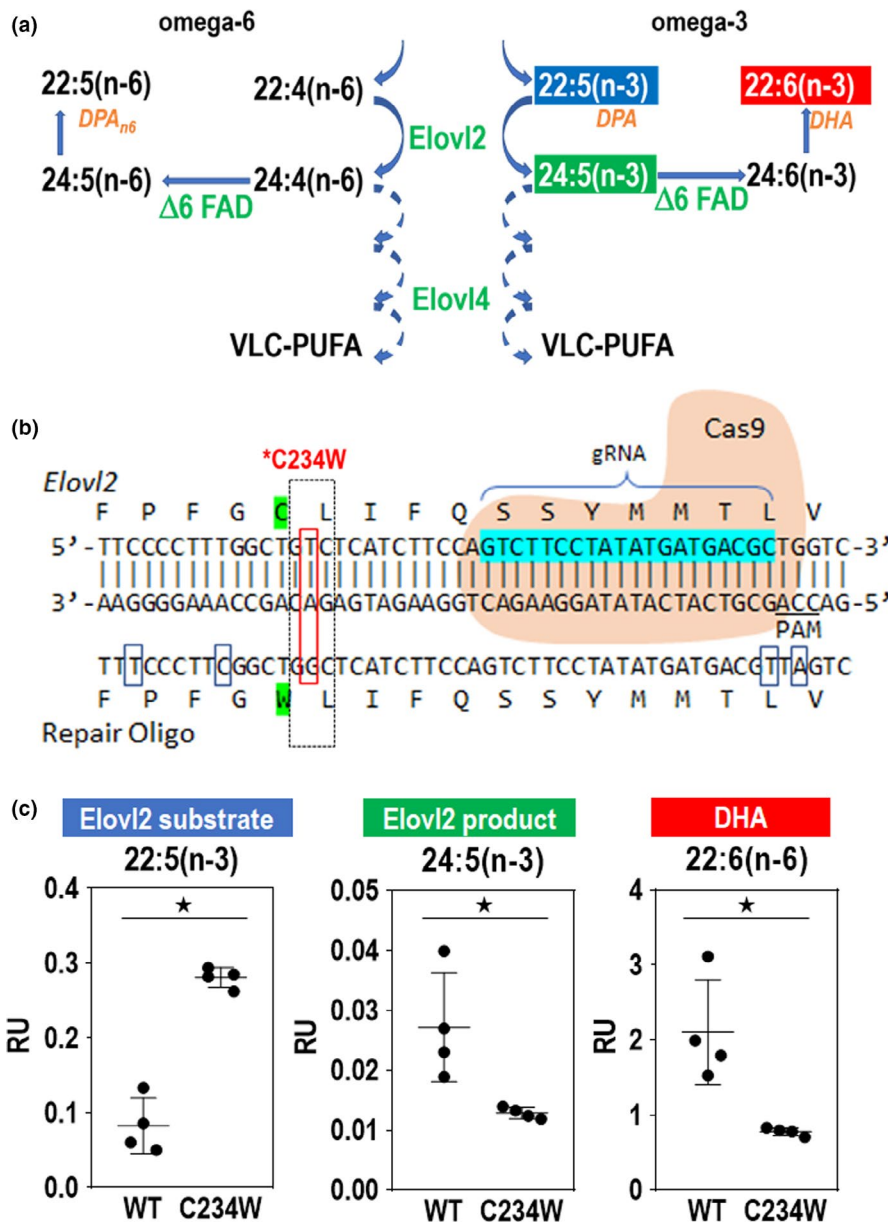
FIGURE 3 *Elovl2*[C234W] mice show a loss of ELOVL2 enzymatic activity. (a) Schematic of ELOVL2 elongation of omega-3 and omega-6 fatty acids. ELOVL2 substrates 22:5 (n-3) and 22:4(n-6) are elongated by ELOVL2 to 24:5(n-3) and 24:4(n-6). This leads to other products such as DHA, DPA$_{n6}$, and VLC-PUFAs, which are elongated by ELOVL4. (b) CRISPR-Cas9 strategy to create *Elovl2*[C234W] mice. *Elovl2* gRNA, Cas9, and repair oligo are used to create the *Elovl2*[C234W] mutant. (c) Lipid levels of ELOVL2 substrate DPA (22:5(n-3)), ELOVL2 product (24:5(n-3)), and DHA (22:6(n-3)) in retinas of *Elovl2*[C234W] mice and wild-type littermates. $N = 4$, *$p < .05$ by Mann–Whitney U test. Error bars represent *SD*

Elovl2[C234W] mice displayed a decrease in visual function as compared to wild-type littermates (Figure 4c, Figure S5).

To determine the impact of the mutation on the morphology of the retina on the microscopic level, we performed an immunohistological analysis of tissue isolated from wild-type and *Elovl2*[C234W] littermates. Although we did not observe gross changes in morphology of the retinas in mutant animals, we have observed the presence of small aggregates underneath the RPE and found that these sub-RPE aggregates contained the complement component C3 as well as the C5b-9 membrane attack complex, proteins found in human drusenoid aggregates (Figure 4d). In addition, in the mutant sub-RPE aggregates, we also identified other components found in human deposits such as HTRA1 (Cameron, 2007), oxidized lipids/ T15 (Shaw, 2012), and ApoE, an apolipoprotein component of drusen (Li, Clark, Chimento, & Curcio, 2006; Figure 4e). This suggests that the sub-RPE deposits found in the *Elovl2*[C234W] mouse contain some drusen-specific components found in early nonexudative AMD. Taken together, these data implicate ELOVL2-specific activity as a potential functional target in age-related eye diseases.

3 | DISCUSSION

3.1 | ELOVL2 as a critical regulator of molecular aging in the retina

This work is the first demonstration, to our knowledge, of a functional role for *Elovl2* in regulating age-associated phenotypes in the retina. Methylation of the promoter region of *ELOVL2* is well-established as a robust prognostic biomarker of human aging (Garagnani, 2012; Gopalan, 2017), but whether ELOVL2 activity contributes to aging phenotypes had not yet been documented.
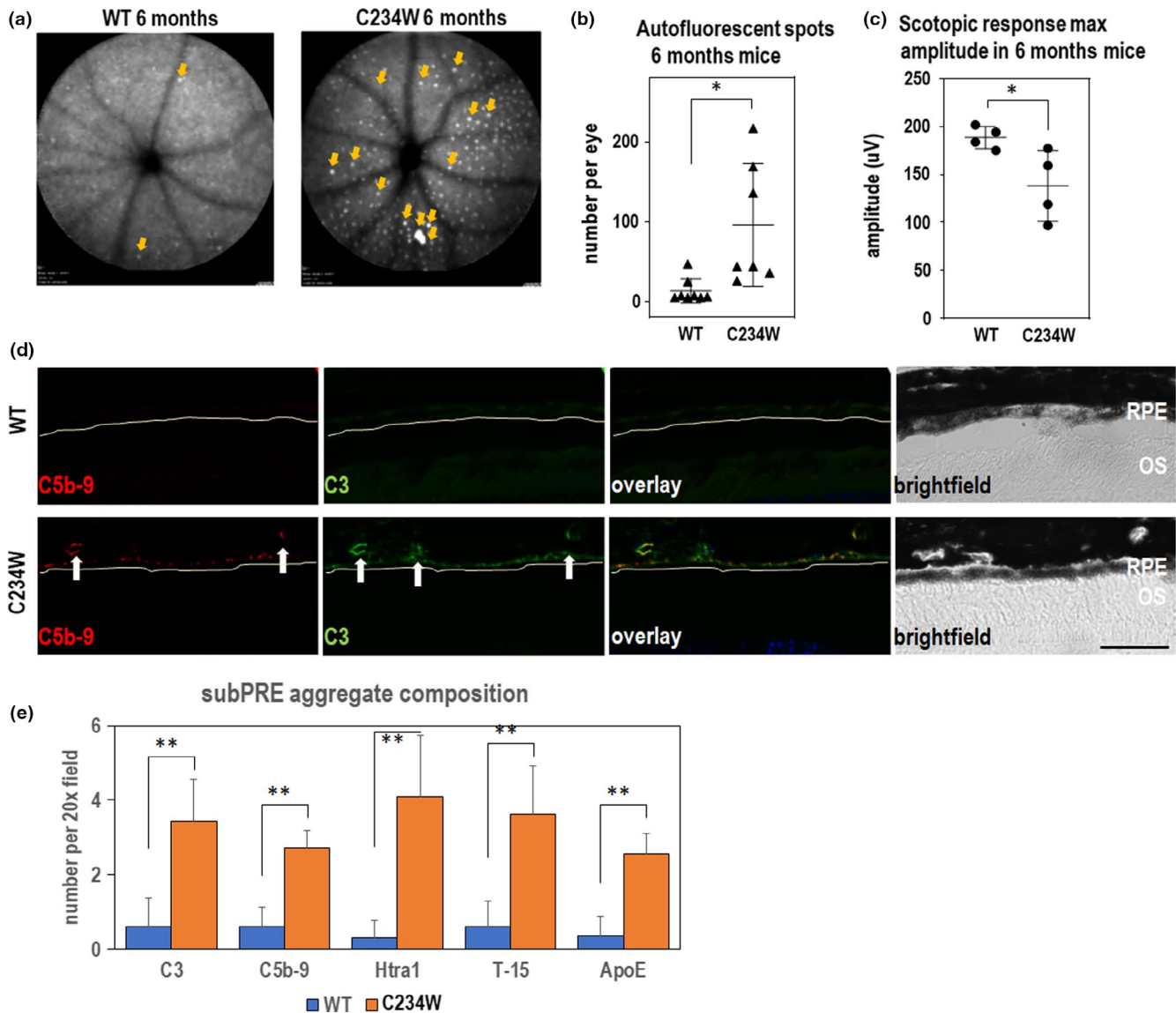
FIGURE 4 *Elovl2*^C234W mice show autofluorescent deposits and vision loss. (a) Representative fundus autofluorescence images of WT and *Elovl2*^C234W mice at 6 months with representative scotopic ERG waveforms. Note multiple autofluorescent deposits (arrows) in *Elovl2*^C234W mice which are almost absent in wild-type littermates. (b) Quantification of the autofluorescent spots in 6mo wild-type and C234W mutant mice. $N = 8$. *$p < .05$, t test. Error bars denote *SD*. (c) Maximum scotopic amplitude by ERG at 6 months between WT and *Elovl2*^C234W mice. $N = 4$, *$p < .05$, t test. Error bars represent *SD*. (d) Immunohistochemistry of sub-RPE deposits found in *Elovl2*^C234W mice. Deposits are found underneath the RPE (yellow line), which colocalize with C3 and C5b-9, which is not present in WT controls. Bar—50um. (e) Quantification of sub-RPE aggregates stained with C3, C5b-9, Htra1, T-15, and ApoE, all components found in drusen in AMD. $N = 4$, **$p < .01$, t test. Error bars represent *SD*

In this work, we demonstrated that the age-related methylation of regulatory regions of *Elovl2* occurs in the rodent retina and results in age-related decreases in the expression of *Elovl2*. We show that inhibition of *ELOVL2* expression by transfection of *ELOVL2* shRNA in two widely used cell models results in increased senescence and decreased proliferation, endpoints associated with aging. Conversely, we show that the administration of 5-Aza-dc leads to demethylation of *ELOVL2* promoter and prevents cell proliferation and senescence compared with controls.

Next, we explored whether *Elovl2* expression affected age-related phenotypes in vivo. Intravitreal injection of 5-Aza-dc in

rodents increased *Elovl2* expression and reversed age-related changes in visual function by ERG. Next, we showed a decrease in visual function as assessed by ERG as well as increased accumulation of autofluorescent white spots in *Elovl2*^C234W mice, with ELOVL2-specific activity eliminated, compared with littermates controls. These physiologic and anatomical phenotypes are well-established markers of aging in the mouse retina, suggesting that loss of *Elovl2* may be accelerating aging on a molecular level in the retina. Finally, in *Elovl2*^C234W mice, we observed the appearance of sub-RPE deposits, which colocalize with markers found in human drusen in macular degeneration, a pathologic hallmark

of a prevalent age-related disease in the eye. Taken together, we propose that *Elovl2* plays a critical role in regulating a molecular aging in the retina, which may have therapeutic implications for age-related eye diseases.

3.2 | Methylation of the regulatory region as a mechanism of age-dependent gene expression

DNA methylation at the 5-position of cytosine (5-methylcytosine, 5mC) is catalyzed and maintained by a family of DNA methyltransferases (DNMTs) in eukaryotes (Law & Jacobsen, 2010) and constitutes ~2%–6% of the total cytosines in human genomic DNA (28). Alterations of 5mC patterns within CpG dinucleotides within regulatory regions are associated with changes in gene expression (Jones, 1998; Telese, Gamliel, Skowronska-Krawczyk, Garcia-Bassets, & Rosenfeld, 2013). Recently, it has been shown that one can predict human aging using DNA methylation patterns. In particular, increased DNA methylation within the CpG island overlapping with the promoter of *ELOVL2* was tightly correlated with the age of the individual (Gopalan, 2017). We attempted to demethylate this region using 5-Aza-dc, known to inhibit the function of DNMTs also in nondividing neurons (Choi et al., 2018; Miller & Sweatt, 2007; Wang, 2018). We reported that upon intravitreal injection of the compound, the DNA methylation is reduced, gene expression is upregulated, and visual function is maintained in the treated eye compared with the contralateral control. These data suggest that *Elovl2* is actively methylated by enzymes inhibited by 5-Aza-dc and that age-related methylation either directly or indirectly regulates *Elovl2* expression. Further studies are needed to fully address the directness and specificity of methylation effects on *Elovl2* expression and visual function.

3.3 | A molecular link between long-chain PUFAs in age-related eye diseases

Our data show that *Elovl2*[C234W] animals display accelerated loss of vision and the appearance of macroscopic autofluorescent spots in fundus images. The exact identity of such spots in mouse models of human diseases is unclear, as they have been suggested to be either protein-rich, lipofuscin deposits or accumulating microglia (Chavali, 2011; Combadiere, 2007). Rather than deciphering the identity of these macroscopic spots, we used the phenotype as a potential sign of age-related changes in the retina, as suggested by others (Chavali, 2011; Kim, 2014).

The composition of aggregates visible on the microscopic level in sub-RPE layers in the retina is potentially informative with regard to human parallels. Using immunofluorescence, we observed the accumulation of several proteins described previously as characteristic for drusen in human AMD samples. Although our analysis did not exhaust the documented components of drusen in human disease (Crabb, 2014), nevertheless, our data show the appearance of these sub-RPE deposits, even in the absence of known confounding mutations or variants correlating with the risk of the disease.

What may be the mechanism by which *Elovl2* activity results in drusen-like deposits and loss of visual function? ELOVL2 plays an essential role in the elongation of long-chain (C22 and C24) omega-3 and omega-6 polyunsaturated acids (LC-PUFAs) (Figure 3a). LC-PUFAs are found primarily in the rod outer segments and play essential roles in retinal function. These PUFAs include both long-chain omega-3 (n-3) and omega-6 (n-6) fatty acids such as docosahexaenoic acid (DHA) and arachidonic acid (AA). DHA is the major polyunsaturated fatty acid found in the retina and has been shown to play diverse roles in photoreceptor function, protection in oxidative stress, and retinal development (Leeuwen, 2018). While DHA has been well-studied in the human retina, the function of other LC-PUFAs in the ELOVL2 elongation pathway is unknown. Further experiments to dissect the roles of specific LC-PUFAs in this pathway and which of these lipid species are implicated in this phenotype are still required.

Multiple lines of evidence have linked PUFAs to age-related macular degeneration (AMD). AMD is the leading cause of blindness in developed countries (Ambati & Fowler, 2012) among the elderly. There are two advanced subtypes of AMD, an exudative form due to neovascularization of the choroidal blood vessels, and a nonexudative form which results in gradual retinal pigment epithelium (RPE) atrophy and photoreceptor death. While there are currently effective therapies for exudative AMD, there are no treatments which prevent photoreceptor death from nonexudative AMD. A pathologic hallmark of nonexudative AMD is the presence of drusen, lipid deposits found below the RPE, which leads to RPE atrophy and photoreceptor death, termed geographic atrophy. The pathogenesis of macular degeneration is complex and with multiple pathways implicated including complement activation, lipid dysregulation, oxidative stress, and inflammation (Ambati & Fowler, 2012). Despite intense research, the age-related molecular mechanisms underlying drusen formation and geographic atrophy are still poorly understood.

Analysis of AMD donor eyes showed decreased levels of multiple LC-PUFAs and VLC-PUFAs in the retina and RPE/choroid compared with age-matched controls (Liu, Chang, Lin, Shen, & Bernstein, 2010). Epidemiologic studies suggest that low dietary intake of LC-PUFAs such as omega-3 fatty acids was associated with a higher risk of AMD (Sangiovanni, 2009; Seddon, George, & Rosner, 2006). Furthermore, mutations in ELOVL4, a key enzyme in the synthesis of VLC-PUFAs, have been identified in Stargardt-like macular dystrophy (STGD3), a juvenile retinal dystrophy with macular deposits reminiscent of AMD (Bernstein, 2001; Edwards, Donoso, & Ritter, 2001; Zhang, 2001). Despite the biochemical, epidemiologic, and genetic evidence implicating PUFAs in AMD, the molecular mechanisms by which LC and VLC-PUFAs are involved in drusen formation and AMD pathogenesis are still poorly understood. The finding that loss of ELOVL2 activity results in early accumulation of sub-RPE deposits strengthens the relationship between PUFAs and macular degeneration. Since *Elovl2* is expressed in both photoreceptors and RPE, whether these phenotypes of visual loss and sub-RPE deposits are due to cell-autonomous function in the photoreceptors and RPE, respectively, or require interplay between photoreceptors and RPE still needs to be established.

3.4 | Role of *Elovl2* in aging

DNA methylation of the regulatory region of *Elovl2* gene is well-established to be a cell-type-independent molecular aging clock (Garagnani, 2012; Hannum, 2013; Slieker, Relton, Gaunt, Slagboom, & Heijmans, 2018) with *Elovl2* expression detectable in many tissues and highest levels observed in liver, testis, and central nervous system including retina (https://www.proteinatlas.org). The high metabolic activity and critical role of PUFAs, reflecting a high metabolic demand for the products of the ELOVL2 enzyme in the photoreceptors, is the most probably the reason why the ocular phenotype is first to be observed in the *Elovl2*[C234W] animals. Further studies are required to establish the role of the gene in other tissues than the retina and impact of the lack of the ELOVL2 products in the lipid bilayers in aged organisms.

4 | CONCLUSIONS

In summary, we have identified the lipid elongation enzyme ELOVL2 as a critical component in regulating molecular aging in the retina. Further studies may lead to a better understanding of molecular mechanisms of aging in the eye, as well as lead to therapeutic strategies to treat a multitude of age-related eye diseases.

5 | METHODS

5.1 | Cell culture and treatment

WI38 (ATCC Cat# CCL-75, RRID:CVCL_0579) and IMR-90 (ATCC Cat# CCL-186, RRID:CVCL_0347) human fibroblasts were cultured in EMEM (ATCC) supplemented with 10% fetal bovine serum (Omega) and 1% penicillin/streptomycin (Gibco), and kept in a humidified incubator at 5% CO_2 and 37°C. Confluence was calculated via ImageJ imaging software, including three fields of view per sample (10×). Upon confluence, cells were split and seeded at a 1:3 ratio. Population doublings (PDs) were calculated by cell count. Knockdown lentivirus was generated using MISSION shRNA (Sigma) according to the manufacturer's instructions. 5-Aza-2'-deoxycytidine was purchased from TSZ Chem (CAS#2353-33–5) and dissolved in cell culture medium at a concentration of 2μM. Cells were treated every day for a period of 48 hr. The medium was then replaced with regular cell culture medium, and the cells were cultured for 5 more days.

5.2 | Senescence-associated β-galactosidase (SA-β-gal) activity

The SA-β-gal activity in cultured cells was determined using the Senescence β-Galactosidase Staining Kit (Cell Signaling Technology), according to the manufacturer's instructions. Cells were stained with DAPI afterward, and percentages of cells that stained positive were calculated with imaging software (Keyence), including three fields of view (10×).

5.3 | Nucleic acid analysis

DNA and RNA were isolated from human fibroblasts and mouse tissues with TRIzol (Ambion) according to the manufacturer's instructions. RNA was converted to cDNA with iScript cDNA Synthesis Kit (Bio-Rad). qPCR was performed using SsoAdvanced Universal SYBR Green Supermix (Bio-Rad).

Methylated DNA immunoprecipitation (MeDIP) was performed by shearing 1μg DNA by Bioruptor (Diagenode) for 8 cycles on the high setting, each cycle consisting of 30 s on and 30 s off. Sheared DNA was denatured, incubated with 1 μg 5mC antibody MABE146 (Millipore) for 2 hr, and then with SureBeads protein G beads (Bio-Rad) for 1 hr. After washing, DNA was purified with QIAquick PCR Purification Kit (Qiagen). qPCR was then performed as above. List of primers can be found in Table S1.

5.4 | Western blotting

10μg of total protein isolated with TRIzol (Invitrogen) from retinas of WT mice of varying stages of development was subject to SDS-PAGE followed by Western blotting (see Table S2 for antibodies used in the study). H3 served as loading control.

5.5 | Quantification of western blots

WB ECL signals were imaged using Bio-Rad ChemiDoc system. Background-subtracted signal intensities were calculated using ImageJ separately for ELOVL2 bands and H3 loading-control bands. ELOVL2 levels were calculated by dividing ELOVL2 signals by corresponding H3 signals, and then normalized to E15.5.

5.6 | RNAscope® In situ hybridization

In situ hybridization was performed using the RNAscope® Multiplex Fluorescent Assay v2 (ACD Diagnostics). Mouse *Elovl2 Rpe65* and *Arr3* probes (p/n 542711, p/n 410151, and p/n 486551, respectively) were designed by the manufacturer. Briefly, fresh frozen histologic sections of mouse eyes were pretreated per manual using hydrogen peroxide and target retrieval reagents such as protease IV. Probes were then hybridized according to the protocol and then detected with TSA Plus® Fluorophores fluorescein, cyanine 3, and cyanine 5 (Perkin Elmer). Sections were mounted with DAPI and Prolong Gold Antifade (Thermo Fisher) with coverslip for imaging and imaged (Keyence BZ-X700).

5.7 | CRISPR-Cas9 design

CRISPR-Cas9 reagents were generated essentially as described (Wang, 2013) and validated in our facility (Concepcion, Ross, Hutt, Yeo, & Hamilton, 2015). T7 promoter was added to cloned Cas9 coding sequence by PCR amplification. The T7-Cas9 product was then gel-purified and used as the template for in vitro transcription (IVT) using mMESSAGE mMACHINE T7 ULTRA Kit (Life Technologies). T7 promoter and sgRNA sequence were synthesized as a long oligonucleotide (Ultramer, IDT) and amplified by PCR. The T7-sgRNA PCR product was gel-purified and used as the template for IVT using the MEGAshortscript T7 Kit (Life Technologies). A repair template encoding the C234W variant was synthesized as a single-stranded oligonucleotide (Ultramer, IDT) and used without purification. Potential off-targets were identified using Cas-OFFinder (Bae, Park, & Kim, 2014), selecting sites with fewest mismatches (http://www.rgenome.net/cas-offinder/). The founder mouse and all F1 mice were sequenced for off-targets. List of primers is in Table S1.

5.8 | Animal injection and analysis

All animal procedures were conducted with the approval of the Institutional Animal Care Committee at the University of California, San Diego (protocol number: S17114). All studies were performed on equal number of females and males. Number of animals nedeed for each experiment was estimated using power analysis.

5.9 | CRISP/Cas9 injection

C57BL/6N mouse zygotes were injected with CRISPR-Cas9 constructs. Oligos were injected into the cytoplasm of the zygotes at the pronuclei stage. Mice were housed on static racks in a conventional animal facility and were fed ad libitum with Teklad Global 2020X diet.

5.10 | Genotyping, mice substrains

To test for the potentially confounding Rd8 mutation, a mutation in the *Crb1* gene which can produce ocular disease phenotypes when homozygous, we sequenced all mice in our study for Rd8. C57BL/6J mice in the aging part of the study were purchased from the Jax Laboratory and confirmed to be negative for mutation in *Crb1* gene. All C234W mutant animals and their littermates were heterozygous for Rd8 mutation. To test RPE65 gene, all animals were tested for the presence of the variants. All animals in the study harbor homozygous RPE65 variant Leu/Leu.

5.11 | Intravitreal injections

For the 5-Aza-dc injection study, mice were anesthetized by intraperitoneal injection of ketamine/xylazine (100 mg/kg and 10 mg/kg, respectively), and given an analgesic eye drop of proparacaine (0.5%, Bausch & Lomb). Animals were intraocularly injected with 1μl of PBS in one eye, and 1 μl of 2 μM 5-Aza-dc dissolved in PBS in the contralateral eye, every other week over a period of 3 months. Drug dosage was estimated based on our cell line experiments and on previously published data (Gore, 2018).

Autofluorescence imaging was performed using the Spectralis ® HRA + OCT scanning laser ophthalmoscope (Heidelberg Engineering) as previously described (16) using blue light fluorescence feature (laser at 488 nm, barrier filter at 500 nm). Using a 55-degree lens, projection images of 10 frames per fundus were taken after centering around the optic nerve. The image that was most in focus was on the outer retina was then quantified blindly by two independent individuals.

Electroretinograms (ERGs) were performed following a previously reported protocol (Luo, 2014). Briefly, mice were dark-adapted for 12 hr, anesthetized with a weight-based intraperitoneal injection of ketamine/xylazine, and given a dilating drop of tropicamide (1.5%, Alcon) as well as a drop of proparacaine (0.5%, Bausch & Lomb) as analgesic. Mice were examined with a full-field Ganzfeld bowl setup (Diagnosys LLC), with electrodes placed on each cornea, with a subcutaneous ground needle electrode placed in the tail, and a reference electrode in the mouth (Grass Telefactor, F-E2). Lubricant (Goniovisc 2.5%, HUB Pharmaceuticals) was used to provide contact of the electrodes with the eyes. Amplification (at 1–1,000 Hz bandpass, without notch filtering), stimuli presentation, and data acquisition are programmed and performed using the UTAS-E 3000 system (LKC Technologies). For scotopic ERG, the retina was stimulated with a xenon lamp at −2 and −0.5 log cd·s/m^2. For photopic ERG, mice were adapted to a background light of 1 log cd·s/m^2, and light stimulation was set at 1.5 log cd·s/m^2. Recordings were collected and averaged in manufacturer's software (Veris, EDI) and processed in Excel.

5.12 | Immunostaining

Eyeballs were collected immediately after sacrificing mice, fixed in 4% paraformaldehyde for 2 hr, and stored in PBS at 4°C. For immunostainings, eyeballs were sectioned, mounted on slides, and then incubated with 5% BSA 0.1% Triton-X PBS blocking solution for 1 hr. Primary antibodies (see Table S2 for antibodies used in the study) were added 1:50 in 5% BSA PBS and incubated at 4°C for 16 hr. Following 3× PBS wash, secondary antibodies were added 1:1,000 in 5% BSA PBS for 30 min at room temperature. Samples were then washed 3x with PBS, stained with DAPI for 5 min at room temperature, mounted, and imaged (Keyence BZ-X700).

5.13 | Lipid analysis

Lipid extraction was performed by homogenization of tissues in a mixture of 1 ml PBS, 1 ml MeOH, and 2 ml CHCl3. Mixtures were vortexed and then centrifuged at 2,200 g for 5 min to separate the aqueous and organic layer. The organic phase containing

the extracted lipids was collected and dried under N2 and stored at −80°C before LC-MS analysis. Extracted samples were dissolved in 100 µl CHCl3; 15 µl was injected for analysis. LC separation was achieved using a Bio-Bond 5U C4 column (Dikma). The LC solvents were as follows: buffer A, 95:5 water:methanol + 0.03% NH4OH; buffer B, 60:35:5 isopropanol:methanol: water + 0.03% NH4OH. A typical LC run consisted of the following for 70 min after injection: 0.1 ml/min 100% buffer A for 5 min, 0.4 ml/min linear gradient from 20% buffer B to 100% buffer B over 50 min, 0.5 ml/min 100% buffer B for 8 min and equilibration with 0.5 ml/min 100% buffer A for 7 min. FFA analysis was performed using a Thermo Scientific Q Exactive Plus fitted with a heated electrospray ionization source. The MS source parameters were 4kV spray voltage, with a probe temperature of 437.5°C and capillary temperature of 268.75°C. Full-scan MS data were collected with a resolution of 70k, AGC target 1x106, max injection time of 100 ms, and scan range 150–2000 m/z. Data-dependent MS (top 5 mode) was acquired with a resolution of 35 k, AGC target 1×105, max injection time of 50 ms, isolation window 1 m/z, scan range 200 to 2,000 m/z, and stepped normalized collision energy (NCE) of 20, 30, and 40. Extracted ion chromatograms for each FFA were generated using a m/z ± 0.01 mass window around the calculated exact mass (i.e., palmitic acid, calculated exact mass for M-H is 255.2330 and the extracted ion chromatogram was 255.22–255.24). Quantification of the FFAs was performed by measuring the area under the peak and is reported as relative units (R.U.).

5.14 | Analysis of ELOVL2 promoter DNA methylation in mice and humans

Reduced representation bisulfite sequencing (RRBS) in mouse blood was downloaded from Gene Expression Omnibus (GEO) using accession number GSE80672 (Petkovich, 2017). For each sample, reads obtained from sequencing were verified using FastQC (Andrews 2010), then trimmed 4bp using TrimGalore (Bioinformatics B 2016) (4bp), and aligned to a bisulfite-converted mouse genome (mm10, Ensembl) using Bismark (v0.14.3) (Krueger & Andrews, 2011), which produced alignments with Bowtie2 (v2.1.0) (Langmead, Trapnell, Pop, & Salzberg, 2009) with parameters "-score_min L,0,-0.2." Methylation values for CpG sites were determined using MethylDackel (v0.2.1).

To explore methylation of the promoter region of ELOLV2, we first designated the promoter as −1000bp to + 300bp with respect to the strand and transcription start site (TSS) and then identified profiled methylation CpGs using BEDtools (v2.25.0) (Quinlan & Hall, 2010). We then binned each profiled CpG in the promoter region according to 30-bp nonoverlapping windows considering CpGs with at least 5 reads. We then grouped the 136 C57BL/6 control mice according to five quantile age bins and took the average methylation for each age bin and each window. All analysis was performed using custom python (version 3.6) scripts, and plots were generated using matplotlib and seaborn.

To explore the homologous region in humans, we accessed human blood methylome data generated using the Human Illumina methylome array downloaded from GEO, using accessions GSE36054 (Alisch, 2012) and GSE40279 (Hannum, 2013) for a total of 736 samples. Methylation data were quantile-normalized using Minfi, (Aryee, 2014) and missing values were imputed using the Impute package in R. These values were adjusted for cell counts as previously described (Gross, 2016). To enable comparisons across different methylation array studies, we implemented beta-mixture quantile dilation (BMIQ; Gross, 2016; Teschendorff, 2013) and used the median of the Hannum et al. dataset as the gold standard (Hannum, 2013).

We then identified probes within the promoter region of ELOLV2 in the human reference (hg19, UCSC), identifying 6 total probes in the commonly profiled region. We then grouped the 787 individuals according to 5 quantile age bins and grouped probes into 10bp nonoverlapping windows. These data were then analyzed and plotted identically as for mice.

CONFLICT OF INTEREST
DSK and DC are scientific cofounders of Visgenx.

AUTHOR CONTRIBUTIONS
D.S.K. designed the study with the contribution of D.C., D.L.C., and K.Z. D.C. performed most of the experiments. L.R. and V.A.N.H. performed animal experiments. D.L.C. and M.D. performed RNAscope analysis. D.L.C., M.Kolar, and A.S. performed lipidomic studies. M. Krawczyk, M. Jafari, and M. Jabari performed additional experiments in the study. M. Krawczyk performed a statistical analysis of the data. T.W. contributed a bioinformatic analysis of the methylation data. K.D.R. and B.A.H. proposed and constructed the Elovl2[C234W] mouse mutation. D.C., D.L.C., and D.S.K. wrote the manuscript with helpful edits from B.A.H.

DATA AVAILABILITY STATEMENT
The data that support the findings of this study are openly available in Dryad at https://doi.org/10.6075/J0TX3CQ9

ORCID
Dorota Skowronska-Krawczyk iD https://orcid.org/0000-0002-5758-4225

REFERENCES

Alisch, R. S., Barwick, B. G., Chopra, P., Myrick, L. K., Satten, G. A., Conneely, K. N., & Warren, S. T. (2012). Age-associated DNA methylation in pediatric populations. *Genome Research*, 22, 623–632. https://doi.org/10.1101/gr.125187.111

Ambati, J., & Fowler, B. J. (2012). Mechanisms of age-related macular degeneration. *Neuron*, 75, 26–39. https://doi.org/10.1016/j.neuron.2012.06.018

Andrews, S. (2010). FastQC: a quality control tool for high throughput sequence data. Retrieved from http://www.bioinformatics.babraham.ac.uk/projects/fastqc.

Aryee, M. J., Jaffe, A. E., Corrada-Bravo, H., Ladd-Acosta, C., Feinberg, A. P., Hansen, K. D., & Irizarry, R. A. (2014). Minfi: A flexible and comprehensive Bioconductor package for the analysis of Infinium DNA methylation microarrays. *Bioinformatics*, 30, 1363–1369. https://doi.org/10.1093/bioinformatics/btu049

Bae, S., Park, J., & Kim, J. S. (2014). Cas-OFFinder: A fast and versatile algorithm that searches for potential off-target sites of Cas9 RNA-guided endonucleases. *Bioinformatics*, 30, 1473–1475. https://doi.org/10.1093/bioinformatics/btu048

Bazan, N. G., Molina, M. F., & Gordon, W. C. (2011). Docosahexaenoic acid signalolipidomics in nutrition: Significance in aging, neuroinflammation, macular degeneration, Alzheimer's, and other neurodegenerative diseases. *Annual Review of Nutrition*, 31, 321–351. https://doi.org/10.1146/annurev.nutr.012809.104635

Bernstein, P. S., Tammur, J., Singh, N., Hutchinson, A., Dixon, M., Pappas, C. M., … Allikmets, R. (2001). Diverse macular dystrophy phenotype caused by a novel complex mutation in the ELOVL4 gene. *Investigative Ophthalmology & Visual Science*, 42, 3331–3336.

Bioinformatics B (2016). Trim Galore! Retrieved from http://www.bioinformatics.babraham.ac.uk/projects/trim_galore/.

Birch, D. G., & Anderson, J. L. (1992). Standardized full-field electroretinography. Normal values and their variation with age. *Archives of Ophthalmology*, 110, 1571–1576. https://doi.org/10.1001/archopht.1992.01080230071024

Cameron, D. J., Yang, Z., Gibbs, D., Chen, H., Kaminoh, Y., Jorgensen, A., … Zhang, K. (2007). HTRA1 variant confers similar risks to geographic atrophy and neovascular age-related macular degeneration. *Cell Cycle*, 6, 1122–1125. https://doi.org/10.4161/cc.6.9.4157

Chavali, V. R. M., Khan, N. W., Cukras, C. A., Bartsch, D.-U., Jablonski, M. M., & Ayyagari, R. (2011). A CTRP5 gene S163R mutation knock-in mouse model for late-onset retinal degeneration. *Human Molecular Genetics*, 20, 2000–2014. https://doi.org/10.1093/hmg/ddr080

Choi, I. A., Lee, C. S., Kim, H. Y., Choi, D. H., & Lee, J. (2018). Effect of inhibition of DNA methylation combined with task-specific training on chronic stroke recovery. *International Journal of Molecular Sciences*, 19(7), 2019. https://doi.org/10.3390/ijms19072019

Christman, J. K. (2002). 5-Azacytidine and 5-aza-2'-deoxycytidine as inhibitors of DNA methylation: Mechanistic studies and their implications for cancer therapy. *Oncogene*, 21, 5483–5495. https://doi.org/10.1038/sj.onc.1205699

Combadière, C., Feumi, C., Raoul, W., Keller, N., Rodéro, M., Pézard, A., … Sennlaub, F. (2007). CX3CR1-dependent subretinal microglia cell accumulation is associated with cardinal features of age-related macular degeneration. *J Clin Invest*, 117, 2920–2928. https://doi.org/10.1172/JCI31692

Concepcion, D., Ross, K. D., Hutt, K. R., Yeo, G. W., & Hamilton, B. A. (2015). Nxf1 natural variant E610G is a semi-dominant suppressor of IAP-induced RNA processing defects. *PLoS Genetics*, 11, e1005123. https://doi.org/10.1371/journal.pgen.1005123

Crabb, J. W. (2014). The proteomics of drusen. *Cold Spring Harbor Perspectives in Medicine*, 4, a017194. https://doi.org/10.1101/cshperspect.a017194

Edwards, A. O., Donoso, L. A., & Ritter, R. 3rd (2001). A novel gene for autosomal dominant Stargardt-like macular dystrophy with homology to the SUR4 protein family. *Investigative Ophthalmology & Visual Science*, 42, 2652–2663.

Garagnani, P., Bacalini, M. G., Pirazzini, C., Gori, D., Giuliani, C., Mari, D., … Franceschi, C. (2012). Methylation of ELOVL2 gene as a new epigenetic marker of age. *Aging Cell*, 11, 1132–1134. https://doi.org/10.1111/acel.12005

Glei, D. A., Goldman, N., Risques, R. A., Rehkopf, D. H., Dow, W. H., Rosero-Bixby, L., & Weinstein, M. (2016). Predicting survival from telomere length versus conventional predictors: A multinational population-based cohort study. *PLoS ONE*, 11, e0152486. https://doi.org/10.1371/journal.pone.0152486

Gopalan, S., Carja, O., Fagny, M., Patin, E., Myrick, J. W., McEwen, L. M., … Henn, B. M. (2017). Trends in DNA methylation with age replicate across diverse human populations. *Genetics*, 206, 1659–1674. https://doi.org/10.1534/genetics.116.195594

Gore, A. V., Tomins, K. A., Iben, J., Ma, L. I., Castranova, D., Davis, A. E., … Weinstein, B. M. (2018). An epigenetic mechanism for cavefish eye degeneration. *Nature Ecology & Evolution*, 2, 1155–1160. https://doi.org/10.1038/s41559-018-0569-4

Gregory, M. K., Cleland, L. G., & James, M. J. (2013). Molecular basis for differential elongation of omega-3 docosapentaenoic acid by the rat Elovl5 and Elovl2. *Journal of Lipid Research*, 54, 2851–2857. https://doi.org/10.1194/jlr.M041368

Gross, A. M., Jaeger, P. A., Kreisberg, J. F., Licon, K., Jepsen, K. L., Khosroheidari, M., … Ideker, T. (2016). Methylome-wide analysis of chronic HIV infection reveals five-year increase in biological age and epigenetic targeting of HLA. *Molecular Cell*, 62, 157–168. https://doi.org/10.1016/j.molcel.2016.03.019

Hannum, G., Guinney, J., Zhao, L., Zhang, L. I., Hughes, G., Sadda, S. V., … Zhang, K. (2013). Genome-wide methylation profiles reveal quantitative views of human aging rates. *Molecular Cell*, 49, 359–367. https://doi.org/10.1016/j.molcel.2012.10.016

Hayflick, L. (1965). The limited in vitro lifetime of human diploid cell strains. *Experimental Cell Research*, 37, 614–636. https://doi.org/10.1016/0014-4827(65)90211-9

Horvath, S. (2013). DNA methylation age of human tissues and cell types. *Genome Biology*, 14, R115. https://doi.org/10.1186/gb-2013-14-10-r115

Jones, P. L., Jan Veenstra, G. C., Wade, P. A., Vermaak, D., Kass, S. U., Landsberger, N., … Wolffe, A. P. (1998). Methylated DNA and MeCP2 recruit histone deacetylase to repress transcription. *Nature Genetics*, 19, 187–191. https://doi.org/10.1038/561

Kim, S.-Y., Yang, H.-J., Chang, Y.-S., Kim, J.-W., Brooks, M., Chew, E. Y., … Swaroop, A. (2014). Deletion of aryl hydrocarbon receptor AHR in mice leads to subretinal accumulation of microglia and RPE atrophy. *Investigative Ophthalmology & Visual Science*, 55, 6031–6040. https://doi.org/10.1167/iovs.14-15091

Kolesnikov, A. V., Fan, J., Crouch, R. K., & Kefalov, V. J. (2010). Age-related deterioration of rod vision in mice. *Journal of Neuroscience*, 30, 11222–11231. https://doi.org/10.1523/JNEUROSCI.4239-09.2010

Krueger, F., & Andrews, S. R. (2011). Bismark: A flexible aligner and methylation caller for Bisulfite-Seq applications. *Bioinformatics*, 27, 1571–1572. https://doi.org/10.1093/bioinformatics/btr167

Langmead, B., Trapnell, C., Pop, M., & Salzberg, S. L. (2009). Ultrafast and memory-efficient alignment of short DNA sequences to the human genome. *Genome Biology*, 10, R25. https://doi.org/10.1186/gb-2009-10-3-r25

Law, J. A., & Jacobsen, S. E. (2010). Establishing, maintaining and modifying DNA methylation patterns in plants and animals. *Nature Reviews Genetics*, 11, 204–220. https://doi.org/10.1038/nrg2719

Leonard, A. E., Kelder, B., Bobik, E. G., Chuang, L.-T., Lewis, C. J., Kopchick, J. J., … Huang, Y.-S. (2002). Identification and expression

of mammalian long-chain PUFA elongation enzymes. *Lipids*, *37*, 733–740. https://doi.org/10.1007/s11745-002-0955-6

Levine, M. E., Lu, A. T., Quach, A., Chen, B. H., Assimes, T. L., Bandinelli, S., ... Horvath, S. (2018). An epigenetic biomarker of aging for lifespan and healthspan. *Aging (Albany NY)*, *10*, 573–591. https://doi.org/10.18632/aging.101414

Li, C.-M., Clark, M. E., Chimento, M. F., & Curcio, C. A. (2006). Apolipoprotein localization in isolated drusen and retinal apolipoprotein gene expression. *Investigative Opthalmology & Visual Science*, *47*, 3119–3128. https://doi.org/10.1167/iovs.05-1446

Liu, A., Chang, J., Lin, Y., Shen, Z., & Bernstein, P. S. (2010). Long-chain and very long-chain polyunsaturated fatty acids in ocular aging and age-related macular degeneration. *Journal of Lipid Research*, *51*, 3217–3229. https://doi.org/10.1194/jlr.M007518

Luo, J., Baranov, P., Patel, S., Ouyang, H., Quach, J., Wu, F., ... Zhang, K. (2014). Human retinal progenitor cell transplantation preserves vision. *Journal of Biological Chemistry*, *289*, 6362–6371. https://doi.org/10.1074/jbc.M113.513713

Miller, C. A., & Sweatt, J. D. (2007). Covalent modification of DNA regulates memory formation. *Neuron*, *53*, 857–869. https://doi.org/10.1016/j.neuron.2007.02.022

Momparler, R. L. (2005). Pharmacology of 5-Aza-2'-deoxycytidine (decitabine). *Seminars in Hematology*, *42*, S9–16. https://doi.org/10.1053/j.seminhematol.2005.05.002

Pauter, A. M., Olsson, P., Asadi, A., Herslöf, B., Csikasz, R. I., Zadravec, D., & Jacobsson, A. (2014). Elovl2 ablation demonstrates that systemic DHA is endogenously produced and is essential for lipid homeostasis in mice. *Journal of Lipid Research*, *55*, 718–728. https://doi.org/10.1194/jlr.M046151

Petkovich, D. A., Podolskiy, D. I., Lobanov, A. V., Lee, S.-G., Miller, R. A., & Gladyshev, V. N. (2017). Using DNA methylation profiling to evaluate biological age and longevity interventions. *Cell Metabolism*, *25*(4), 954–960.e6. https://doi.org/10.1016/j.cmet.2017.03.016

Quinlan, A. R., & Hall, I. M. (2010). BEDTools: A flexible suite of utilities for comparing genomic features. *Bioinformatics*, *26*, 841–842. https://doi.org/10.1093/bioinformatics/btq033

Sangiovanni, J. P., Agrón, E., Meleth, A. D., Reed, G. F., Sperduto, R. D., Clemons, T. E., ... Age-Related Eye Disease Study Research Group (2009). {omega}-3 Long-chain polyunsaturated fatty acid intake and 12-y incidence of neovascular age-related macular degeneration and central geographic atrophy: AREDS report 30, a prospective cohort study from the Age-Related Eye Disease Study. *American Journal of Clinical Nutrition*, *90*, 1601–1607. https://doi.org/10.3945/ajcn.2009.27594

Seddon, J. M., George, S., & Rosner, B. (2006). Cigarette smoking, fish consumption, omega-3 fatty acid intake, and associations with age-related macular degeneration: The US Twin Study of age-related macular degeneration. *Archives of Ophthalmology*, *124*, 995–1001. https://doi.org/10.1001/archopht.124.7.995

Shaw, P. X., Zhang, L., Zhang, M., Du, H., Zhao, L., Lee, C., ... Zhang, K. (2012). Complement factor H genotypes impact risk of age-related macular degeneration by interaction with oxidized phospholipids. *Proceedings of the National Academy of Sciences USA*, *109*, 13757–13762. https://doi.org/10.1073/pnas.1121309109

Slieker, R. C., Relton, C. L., Gaunt, T. R., Slagboom, P. E., & Heijmans, B. T. (2018). Age-related DNA methylation changes are tissue-specific with ELOVL2 promoter methylation as exception. *Epigenetics Chromatin*, *11*, 25. https://doi.org/10.1186/s13072-018-0191-3

Stempel, A. J., Morgans, C. W., Stout, J. T., & Appukuttan, B. (2014). Simultaneous visualization and cell-specific confirmation of RNA and protein in the mouse retina. *Molecular Vision*, *20*, 1366–1373.

Telese, F., Gamliel, A., Skowronska-Krawczyk, D., Garcia-Bassets, I., & Rosenfeld, M. G. (2013). "Seq-ing" insights into the epigenetics of neuronal gene regulation. *Neuron*, *77*, 606–623. https://doi.org/10.1016/j.neuron.2013.01.034

Teschendorff, A. E., Marabita, F., Lechner, M., Bartlett, T., Tegner, J., Gomez-Cabrero, D., & Beck, S. (2013). A beta-mixture quantile normalization method for correcting probe design bias in Illumina Infinium 450 k DNA methylation data. *Bioinformatics*, *29*, 189–196. https://doi.org/10.1093/bioinformatics/bts680

van Leeuwen, E. M., Emri, E., Merle, B. M. J., Colijn, J. M., Kersten, E., Cougnard-Gregoire, A., ... Lengyel, I. (2018). A new perspective on lipid research in age-related macular degeneration. *Progress in Retinal and Eye Research*, *67*, 56–86. https://doi.org/10.1016/j.preteyeres.2018.04.006

Wang, H., Yang, H., Shivalila, C. S., Dawlaty, M. M., Cheng, A. W., Zhang, F., & Jaenisch, R. (2013). One-step generation of mice carrying mutations in multiple genes by CRISPR/Cas-mediated genome engineering. *Cell*, *153*, 910–918. https://doi.org/10.1016/j.cell.2013.04.025

Wang, Q., Xu, L., Chen, P., Xu, Z., Qiu, J., Ge, J., ... Zhuang, J. (2018). Brca1 Is upregulated by 5-Aza-CdR and promotes DNA repair and cell survival, and inhibits neurite outgrowth in rat retinal neurons. *International Journal of Molecular Sciences*, *19*, https://doi.org/10.3390/ijms19041214

Wang, T., Tsui, B., Kreisberg, J. F., Robertson, N. A., Gross, A. M., Yu, M. K., ... Ideker, T. (2017). Epigenetic aging signatures in mice livers are slowed by dwarfism, calorie restriction and rapamycin treatment. *Genome Biology*, *18*, 57. https://doi.org/10.1186/s13059-017-1186-2

Weber, M., Davies, J. J., Wittig, D., Oakeley, E. J., Haase, M., Lam, W. L., & Schübeler, D. (2005). Chromosome-wide and promoter-specific analyses identify sites of differential DNA methylation in normal and transformed human cells. *Nature Genetics*, *37*, 853–862. https://doi.org/10.1038/ng1598

Williams, G. A., & Jacobs, G. H. (2007). Cone-based vision in the aging mouse. *Vision Research*, *47*, 2037–2046. https://doi.org/10.1016/j.visres.2007.03.023

Xie, W., Baylin, S. B., & Easwaran, H. (2019). DNA methylation in senescence, aging and cancer. *Oncoscience*, *6*, 291–293. https://doi.org/10.18632/oncoscience.476

Xu, H., Chen, M., Manivannan, A., Louis, N., & Forrester, J. V. (2008). Age-dependent accumulation of lipofuscin in perivascular and subretinal microglia in experimental mice. *Aging Cell*, *7*(1), 58–68.

Zadravec, D., Tvrdik, P., Guillou, H., Haslam, R., Kobayashi, T., Napier, J. A., ... Jacobsson, A. (2011). ELOVL2 controls the level of n-6 28:5 and 30:5 fatty acids in testis, a prerequisite for male fertility and sperm maturation in mice. *Journal of Lipid Research*, *52*, 245–255. https://doi.org/10.1194/jlr.M011346

Zhang, K., Kniazeva, M., Han, M., Li, W., Yu, Z., Yang, Z., ... Petrukhin, K. (2001). A 5-bp deletion in ELOVL4 is associated with two related forms of autosomal dominant macular dystrophy. *Nature Genetics*, *27*, 89–93. https://doi.org/10.1038/83817

SUPPORTING INFORMATION

Additional supporting information may be found online in the Supporting Information section.